

Intrinsically disordered region of talin's FERM domain functions as an initial PIP₂ recognition site

Jannik Buhr^{1,2}, Florian Franz^{1,2}, and Frauke Gräter^{1,2,*}

¹Heidelberg Institute for Theoretical Studies

²Interdisciplinary Center for Scientific Computing, Heidelberg University

*Correspondence: Frauke.Graeter@h-its.org

ABSTRACT Focal adhesions (FAs) mediate the interaction of the cytoskeleton with the extracellular matrix (ECM) in a highly dynamic fashion. talin is a central regulator, adaptor protein and mechano-sensor of focal adhesion complexes. For recruitment and firm attachment at FAs, talin's N-terminal FERM domain binds to phosphatidylinositol 4,5-bisphosphate (PIP₂)-enriched membranes. A newly published autoinhibitory structure of talin-1, where the known PIP₂ interaction sites are covered up, lead us to hypothesize that a hitherto less examined loop insertion of the FERM domain acts as an additional and initial site of contact. We evaluated direct interactions of talin-1 with a PIP₂ membrane by means of atomistic molecular dynamics (MD) simulations. We show that this unstructured, 33-residue-long loop strongly interacts with PIP₂ and can facilitate further membrane contacts, including the canonical PIP₂ interactions, by serving as a flexible membrane anchor. Under force as present at FAs, the extensible FERM loop ensures talin to maintain membrane contacts when pulled away from the membrane by up to 7 nm. We identify key basic residues of the anchor mediating the highly dynamic talin-membrane interaction. Our results put forward an intrinsically disordered loop as a key and highly adaptable PIP₂ recognition site of talin and potentially other PIP₂-binding mechano-proteins.

SIGNIFICANCE FERM domains are modular domains that often harbor PIP₂ binding sites and serve as anchoring points to membranes. talin's FERM domain features a peculiar long and disordered loop, the function of which has remained fully elusive. We here show by means of atomistic molecular dynamics simulations that the loop serves as a first PIP₂ interaction site and flexible anchor to the membrane. This provides mechanistic insight into the role of intrinsically disordered regions in protein–membrane interactions.

INTRODUCTION

Tip

This is a draft and as such subject to change. The source repository for this manuscript lives at <https://github.com/hits-mbm-dev/paper-talin-loop>. The manuscript and poster are available in multiple formats:

- manuscript web/html: <https://hits-mbm-dev.github.io/paper-talin-loop/>
- manuscript print/pdf: <https://hits-mbm-dev.github.io/paper-talin-loop/index.pdf>
- poster web/html: <https://hits-mbm-dev.github.io/paper-talin-loop/poster.html>
- poster print/pdf: <https://hits-mbm-dev.github.io/paper-talin-loop/poster.pdf>

Cells critically sense the mechanics of their environment at cell adhesion sites for a multitude of biological processes. Contact with the extracellular matrix and surrounding cells regulates growth, differentiation, motility and even apoptosis (1–4). The multiprotein focal adhesion complex is responsible for translating between and integrating biochemical and mechanical signals for both outside-in and inside-out activation (5, 6).

At the center of the focal adhesion complex sits the adaptor protein talin, which dynamically unfolds and refolds under force (7). A schematic of talin can be seen in Figure 1a. Through interaction with integrin tails (dark green) (8), which in turn interact with collagen fibers via their heads, it links the extracellular matrix to the intracellular cytoskeleton by directly interacting with actin. Talin also features specific interactions with the membrane. Their formation, mechanical stability and role in mechanosensing remain to be fully resolved.

Talin contains an N-terminal FERM domain (F for

4.1 protein, E for ezrin, R for radixin and M for moesin), which is composed of the subdomains F0 to F3 and provides a link to the cytosolic side of the plasma membrane (9). It does so via a conserved binding motif for phosphatidylinositol 4,5-bisphosphate (PIP_2), which is enriched at active focal adhesion sites (10–12). The main PIP_2 binding sites are located in F2 and F3 (highlighted as red spheres in Figure 1a).

Two isoforms exist of talin, talin-1 and talin-2, encoded by the *tln1* and *tln2* genes. This work refers to talin-1 if not otherwise stated. Notably, the talin-1 FERM domain differs from other FERM proteins through the addition of the F0 subdomain, which is connected to F1 via a charged interface, as well as an insertion in F1, a flexible loop with helical propensity and basic residues (13). Additionally, talin's FERM domain exists in an extended conformation, as opposed to the cloverleaf-like conformation of other FERM proteins (14). F3 also has a binding site for β -integrin tails (15) and is partly responsible for the enrichment of PIP_2 at the membrane through a binding site for PIPKI γ (16). A second integrin binding site is located in the rod domain 11 (R11) (17). Talin interacts with the cytoskeleton through actin binding sites (F2-F3, R4-R8, R13-DH) (18). The review by Klapholz et al. (19) provides an excellent overview of the many interaction sites of talin and their central role in the focal adhesion complex.

The mechanistic role of the disordered loop in the F1 domain in the many aspects of talin function remains elusive. Its overall positive charge renders it a prime candidate as a PIP_2 binding site. However, previous studies only identified a minor role of the loop in PIP_2 binding compared to F2-F3 (20, 21). On the other hand, the F1 loop has been shown to contribute to talin-mediated integrin activation (13).

It was previously shown that F3 can interact with R9, which impedes integrin activation (22). Furthermore, in a recently determined cryo-electron microscopy structure of autoinhibited talin-1, Dedden et al. (23) showed that the rod domains R9 and R12 shield the established PIP_2 binding surface and the integrin binding site in F3 (see Figure 1b, Figure 1c). This beckons the question how this autoinhibition can be resolved. Song et al. (12) previously investigated a fragment of talin consisting of F2-F3 and an inhibiting rod segment and suggested a pull-push mechanism, whereby negatively charged PIP_2 attracts its positively charged binding surface on F2-F3 and simultaneously repels the negatively charged surface of the inhibitory rod segment. However, this still leaves open the question of how talin can establish a first contact with the membrane and remain within a sufficient proximity for this effect to kick in.

We hypothesized that the flexible F1 loop inserted

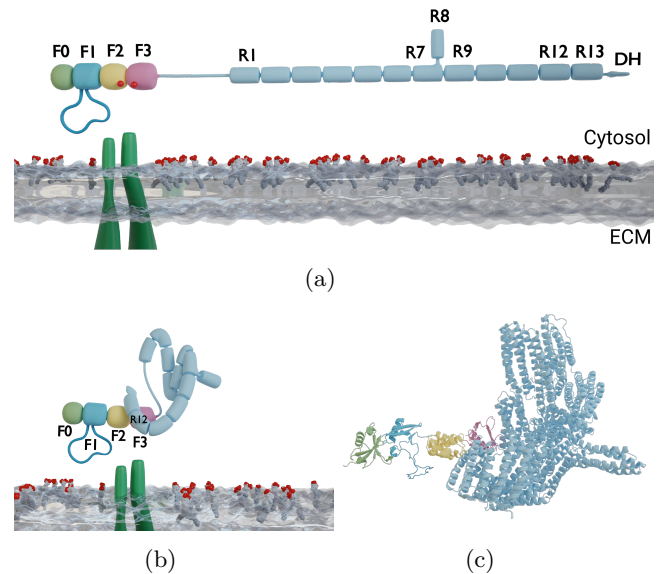


Figure 1: A schematic overview of talin and our simulation setup. **a)** A schematic rendering of full-length talin over a POPC membrane enriched with PIP_2 in the upper, intracellular leaflet. The subdomains under scrutiny in this publication, namely F0-F3, which comprise the N-terminal FERM domain (or talin head), are highlighted in pastel colors (green, cyan, yellow, magenta). The two major PIP_2 binding sites in F2-F3 are marked with red spheres. The talin rod segments (or talin tail) are numbered R1 to R13. Note that under physiological conditions, with talin experiencing force from bound actin, the angle between the FERM domain and the talin rod would be more akin to 30° as opposed to the linear structure shown here for illustrative purposes. Tails of an integrin α and β heterodimer reaching through the lipid bilayer are represented in green. **b)** A schematic rendering of the autoinhibited structure of talin as crystallized by Dedden et al. (23) in combination with a cartoon representation in **c**). The primary PIP_2 binding site of F2-F3 is occluded in talin, while the loops of F1 is accessible, as evident when fitting the F0-F3 structure by Elliott et al. (14), with our addition of the modelled F1 loop, to the autoinhibited structure, which lacks F0F1. The main PIP_2 -binding sites in F2-F3 are occluded by rod domain 12. The complete FERM structure can be explored interactively in the context of our simulation system in the Supplementary Materials.

into talin's FERM domain serves as an additional PIP₂ interaction site. As such it would be readily accessible to PIP₂ even in talin's autoinhibited conformation and would further mechanically stabilize talin's interaction with the membrane. To test this hypothesis, we modelled the loop, which, due to its high flexibility, is not included in crystal structures of the FERM domain, such as PDB-ID 3IVF by Elliot et al. (14).

With a complete structure of the talin FERM domain, we investigated the role of the F1 loop through atomistic molecular dynamics (MD) simulations, which had previously also proven useful to detect the recognition of PIP₂ in membranes by PH domains (24) or the FERM domain of focal adhesion kinase (25).

In F0F1 simulations, we found the loop to have a clear propensity to interact with the PIP₂-containing membrane. It is able to establish a first contact with the membrane even from unfavorable initial orientations due to its large search volume. Furthermore, we show with simulations of the full-length FERM domain that once the loop has established an initial contact, it can anchor the FERM domain to the membrane and allow the known major binding sites in F2-F3 to form.

These results provide mechanistic insight talin-PIP₂ interactions and highlight the role of secondary intrinsically disordered binding surfaces for membrane recognition.

MATERIALS AND METHODS

Molecular dynamics with GROMACS

MD simulations were performed with GROMACS (26, 27) version 2020.03 (28). A crystal structure of the talin FERM domain by Elliot et al. (14) with the PDB-ID 3IVF was used as the basis of all simulations.

The deleted or missing residues (134-172) belonging to the F1 domain loop were modeled using MODELLER (29, 30) via the interface to Chimera (31), followed by equilibration with GROMACS. The resulting conformation was compared to an NMR structure of the F1 domain (PDB-ID 2KC2) by Goult et al. (13). The missing residue M1 was also added. The missing residues D125 and E126 as well as I399 and L400 were not modelled, as they are far from the region of interest (the F1-loop). This leaves us with a sequence from residue 1 to 398 with a shift by 2 in numbering compared to the canonical TLN1_MOUSE talin-1 sequence (uniprot ID P26039) after residue 124. Simulations were performed with the CHARMM36 force field. Topologies, including the membrane, were generated with the CHARMM-GUI web app (32-34) and GROMACS tools. All simulations used the TIP3P water model and were neutralized with 0.15 mol/L of NaCl. A 6-step equilibration was performed after

gradient descent energy minimization. This followed the standard procedure recommended by CHARMM-GUI, where restraints on protein and membrane atoms were gradually relieved in six steps from 1000 and 4000 kJ/mol/nm² for the membrane and protein atoms on time scales of 25-100 ps, followed by 5 ns of equilibration with only protein atoms subjected to 50 kJ/mol/nm² position restraints. The exact Molecular Dynamics Parameter (mdp) files are provided in the data (<https://doi.org/10.11588/data/BQTQUN>) in the assets folder of each simulation system. Production runs used a timestep of 2 fs, a Verlet cut-off scheme for Van-der-Waals interactions and the Particle Mesh Ewald (PME) method for long-range electrostatics. NPT-ensembles were achieved by Nosé-Hoover temperature coupling (35, 36) and Parinello-Rahman pressure coupling (37). An example .mdp-file can be found in the Supplementary Materials.

The initial equilibrium simulation of the completed FERM domain was run for 75 ns. Subsequently, the root mean squared fluctuation (RMSF) was calculated with GROMACS tools (see Supplementary Material Figure 7a and Figure 7b).

The F0F1 FERM sub domains (residues 1 to 197) were simulated to evaluate protein-membrane association using a rotational sampling approach. This entailed placing the protein 1.5 nm away from a 1-palmitoyl-2-oleyl-glycero-3-phosphocholine (POPC) membrane, where 12 of the 119 lipids in the upper leaflet were replaced with PIP₂. This results in a physiological concentration of 10% PIP₂. The PIP₂ molecules used in the simulations have a charge of -4, consistent with the deprotonation state of the phosphate groups at physiological pH (38).

60 different starting orientations of the protein were generated, spanning a rotation of 360 degrees. The protein was rotated in such a way that the respective closest residue had the same distance to the membrane for the 0° and the 180° starting positions. 6 replicates of each orientation were run for 200 ns each. However, due to a hardware failure, 2 of these 360 runs are corrupted and thus excluded from the analysis.

From this rotational sampling, we selected representative conformations with loop-membrane interactions as the basis of 6 equilibrium simulations of the complete FERM domain over a POPC membrane with 26 PIP₂ lipids out of a total of 273 lipids in the upper leaflet. Each simulation ran for 400 ns. The initial conformations for perpendicular pulling simulations of the F0F1 subdomains to gauge interaction strength were also chosen from the rotational sampling set. The pulling simulations used an umbrella potential applied to the C-terminus with a harmonic force constant of 500 kJ/mol/nm² and a constant speed of 0.03 m/s (See Supplementary Data

in f0f1-vert-pulling/pull_00003.mdp)

Distance information was extracted from trajectories with gromacs tools interfaced via CONAN (39).

Automation, Data Analysis and Availability

Setup scripts written in bash are available for all simulations shown in this work. Computations for data analysis were tracked with the targets R package (40). Plots were generated with ggplot2 (41). Interactive structure representations are embedded using Mol* (42). Schematic visualizations were rendered with blender (43) and VMD (44). Files relevant to this work that are too big to be uploaded to this repository, such as trajectories and blender files, will be uploaded to a separate location. This manuscript was generated with quarto (45–47).

RESULTS

The F1 loop can act as a point of first contact

The high flexibility of the F1 loop gave us the confidence to model it from sequence. It retained its flexibility in equilibrium simulations, in close agreement with the conformational flexibility reflected in the NMR ensemble of the F1 domain (13), which confirmed this approach (see Supplementary Material Figure 7a, Figure 7b and Figure 9a with Figure 9b). The resulting system that provides the basis for our simulations can be explored interactively in the Supplementary Materials.

When simulating only F0F1 over a POPC membrane containing 10% PIP₂, we noticed that the F1 loop had a clear propensity to establish contact with the membrane. Once the contact had been established, the protein was anchored strongly enough for more contacts to evolve with time, pulling the protein onto the membrane (Figure 2a). In order to control for a potential bias towards the loop as a result of the starting position, we performed a rotational sampling of the system, where the starting angle of the loop with respect to the membrane was varied across 60 equally spaced angles. Figure 2b shows that independent of the starting position, the loop is able to find the membrane and bind to it. A residue of the F1 loop is likely to be the first to establish membrane contact even in simulations where the loop starts oriented away from the membrane (Figure 8d). This is due to the large search space it can cover with its high flexibility (see Figure 7a). Expectedly, binding happens earlier in the simulation when the loop starts oriented favorably towards the membrane (Figure 3a, 0°) and the time to first contact is shorter for residues of the F1 loop (Figure 8c). While Figure 2a shows one example of a bound conformation, a conformation for

each starting angle can be seen in the [Supplementary Material](#).

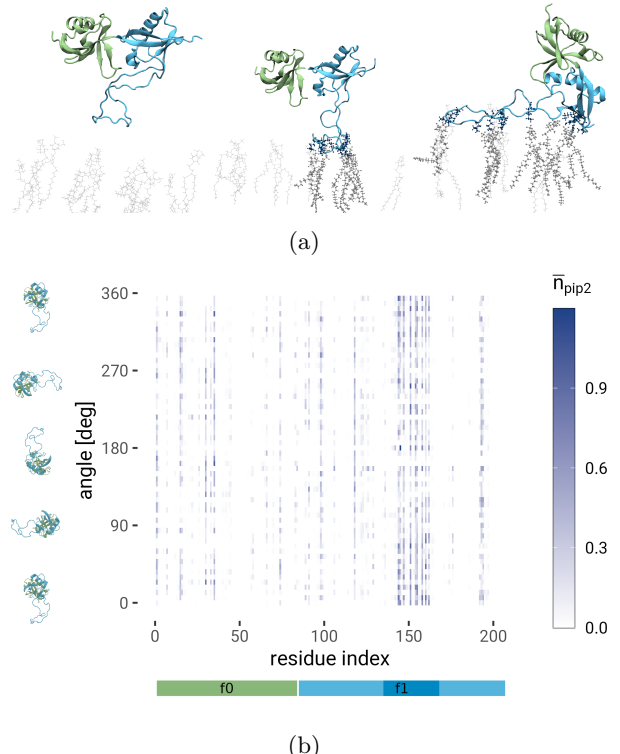


Figure 2: Rotational sampling of F0F1 reveals the lipid binding capabilities of the F1 loop. **a)** Snapshots from a simulation involving F0F1 over a POPC membrane containing 10% PIP₂ in the upper leaflet. POPC is not rendered and PIP₂ is shown as light grey stick models that turn thicker for those molecules that are currently interacting with residues of the protein. The PIP₂-binding residues are then shown as dark blue stick models. **b)** Time-averaged number of PIP₂ molecules bound per residue along the F0F1 sequence (x-axis) as a heatmap summarizing 358 simulations from a rotational sampling, with the starting angle on the y-axis. We sampled 60 different starting positions, rotated equally spaced around the horizontal axis, with 6 replicates each. Each simulation is 200 ns long. 0° corresponds to the loop pointing downwards towards the membrane, as shown in the smaller renders to the left of the heatmap.

Once a contact has been made, it becomes exceedingly unlikely for F0F1 to dissociate from the membrane (Figure 3b). Out of 358 runs¹, 89 runs never made contact with the membrane, but out of the 269 that did, only 10 eventually dissociated. Thus, the simulated timeframe of 200 ns per trajectory allowed for the observation of some reversibility of FERM–PIP₂ binding,

¹ 16 replicas each for 60 angles minus 2 runs lost to a storage failure

albeit only for weakly bound cases and at a small rate of 3.7%. Dissociation from the membrane never occurred on the simulated time scale after more than 3 residues had already made contact.

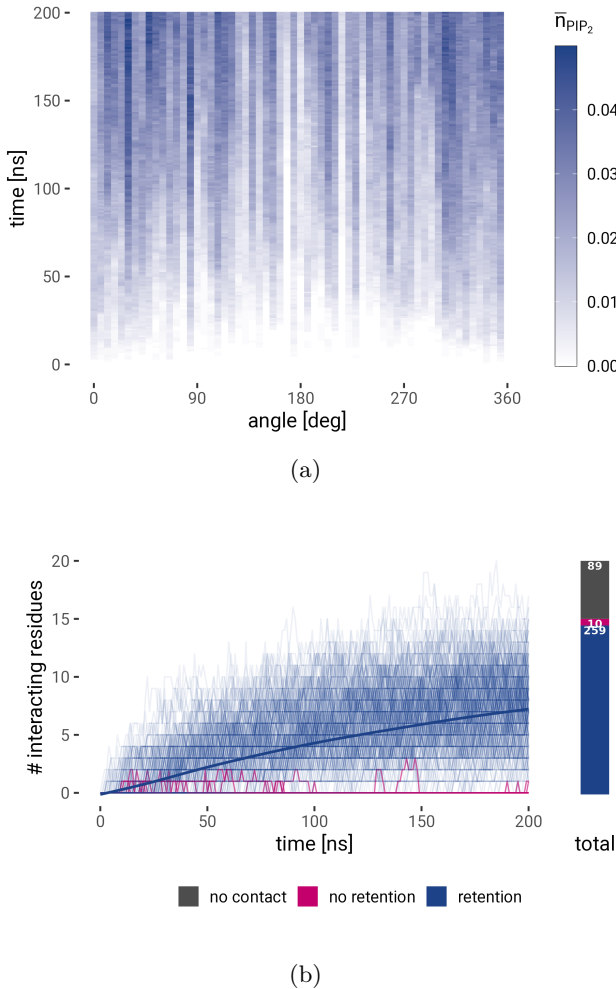


Figure 3: Loop–PIP₂ contacts dynamically accumulate and are mediated by basic residues. **a)** Heatmap of the time evolution of the average number of PIP₂ molecules per residue at the respective time (y-axis) and angle (x-axis). **b)** Time evolution (x-axis) of the number of residues currently interacting with PIP₂ (y-axis) shows binding and unbinding events and an eventual accumulation of contacts. Unbinding becomes exceedingly unlikely as the number of contacts increases.

Figure 4 highlights the residues involved in the interaction of F0F1 with PIP₂. The ensemble of final bound conformations from the simulations can be seen in the [Supplementary Material](#). We observe a number of prominent lysines and arginines, both positively charged residues, across the whole F0F1 fragment to compensate for the negative charge on PIP₂. The

loop region, highlighted with a grey backdrop in Figure 4a, is particularly dense in positively charged residues, albeit the number of PIP₂ contacts per basic residue is only marginally higher in this region than elsewhere. Arginines and lysines in regions outside of the disordered loop complement the binding once initial contacts have been established with the loop, and further strengthen the interaction. F0 at the N-terminus (left) is quite flexible as well (see Figure 7a) and can thus reasonably contribute towards membrane binding. The C-terminus of the F1 domain, instead, harbors the interface towards the F2 domain and the two PIP₂-interacting residues identified here will be more occluded *in vivo*. Indeed, simulations of the full-length FERM domain in the later part of this work do not show these interactions anymore (Figure 6a).

The F1 loop maintains and further facilitates formation of FERM–PIP₂ interactions

To examine the strength of the PIP₂ interactions and the role of the F1 loop in maintaining it, we pulled F0F1 vertically off the membrane in additional force-probe MD simulations (Figure 5). An exemplary render of one of the simulations can be seen in Figure 5a. Pulling F0F1 off the membrane requires peak forces of 100–120 pN, during which the interacting residues only very gradually loose contact (Figure 5), as the high flexibility of F1-loop allows the residues to remain in contact even as the distance increases up to a delta of 7 nm. Replicate 4 stands out as the highest curve (dashed lines), as in this run the interactions were so strong that a total of 3 molecules of PIP₂ were pulled out of the membrane (1 by F0 and 2 by the F1 loop). A snapshot of this can be seen in Figure 8b. This highlights the strong anchoring capabilities of the F1 loop.

As seen in Figure 5c, during pulling residues not belonging to the F1 loop loose contact first, while the loop stays attached. The F1 loop works in conjunction with the F0 subdomain (see Figure 8a). Their high flexibility allows them to remain in contact with the membrane over large distances, which would allow for a spring-like re-establishing of more contacts should the force be alleviated. In two cases the last interacting residue was part of the F1 loop, while in three cases the N-terminus of the F0 domain stayed attached for longest.

Having established the prominent role of the F1-loop in positioning F0F1 at the membrane and establishing PIP₂ contacts, we next examined this role in the larger context of the full FERM domain. 6 independent simulations were initiated with the full-length FERM domain oriented in such that the tip of the F1-loop was in contact with at least one molecule of PIP₂ with varying local environments (see [Simulation Systems and Struc-](#)

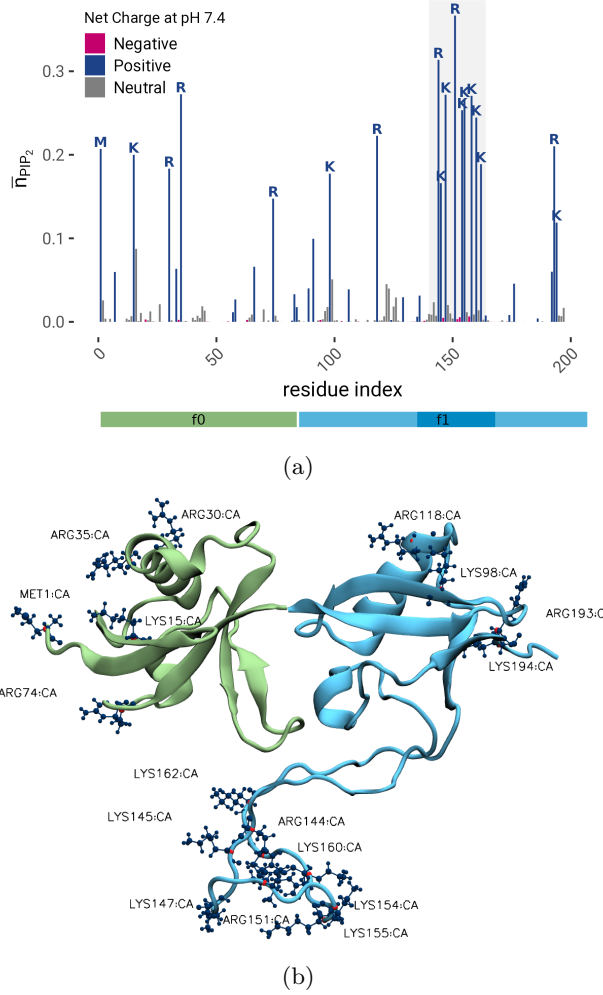


Figure 4: Lysine and arginine residues are crucial for the PIP_2 -interaction of F0F1. **a)** The average number of PIP_2 molecules (\bar{n}_{PIP_2}) interacting (see Figure 7c for the interaction distance definition) with the individual residues per frame across all simulations of the rotational sampling that made contact with the membrane. Color represents the charge of the amino acid at pH 7.4 (blue = positive/basic, magenta = negative/acidic). A number of very prominent lysines can be observed, as well as a cluster of residues belonging to the F1 loop, which is highlighted with a grey backdrop. The most prominent residues are highlighted in **b)**. For the print version it is a snapshot render. The video is also available here: <https://youtu.be/s5yya0XeNTA>.

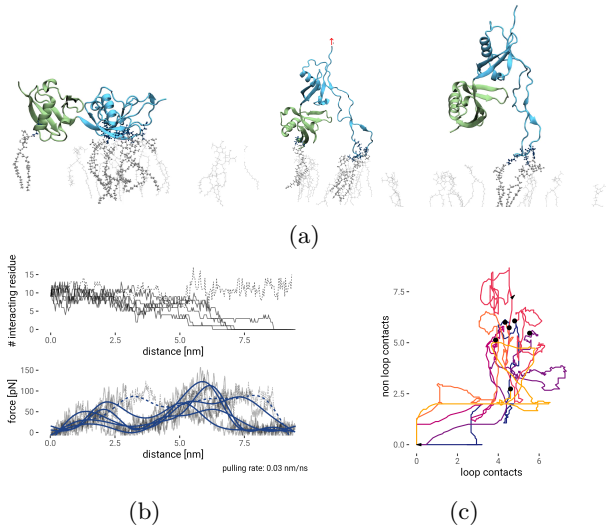


Figure 5: Vertical pulling of F0F1 highlights the F1 loop's flexibility and ability to maintain contacts with the membrane over large distances. **a)** Representative render of one of 6 force-probe MD simulations pulling F0F1 off the membrane. For the print version we show a series of three snapshots, the video is available here: <https://youtu.be/-eZ2orx7QRE>. It starts from a snapshot of F0F1 in its bound conformation taken from the rotational sampling and gets pulled upwards from its C-terminus. **b)** Number of interacting residues (top panel) and the force (bottom panel) as a function of distance (x-axis) as F0F1 gets pulled off the membrane at a constant rate of 0.03 nm/ns. **c)** Time evolution of the number of contacts for residues belonging to the F1 loop (x-axis) and other residues (y-axis). Traces are colored by replicate. Black dots mark the starting positions. The non-loop contacts are mostly supplied by the residues of the F0 N-terminus also shown in Figure 4a.

tures for one example). Individual interaction heatmaps for each run can be found in the Supplementary Material Figure 7d. These simulations highlight the prominent role of the F1-loop in membrane interactions, now in the context of the full-length FERM domain (Figure 6a, compare to Figure 4a). They also reproduce the canonical PIP₂ contacts in F2 and F3 known from previous studies, validating our MD simulations. The highlighted residues include K272 of F2 and K316, K324, E342, and K343 of F3, which have been shown to be crucial for the membrane interaction of talin and subsequent integrin activation by Chinthalapudi et al. (20). Importantly, the loop shows a very dense cluster of PIP₂ interactions, with interaction scores (\bar{n}_{PIP_2}) very similar to these previously known PIP₂-interacting residues. The interacting conformations can be seen in context in the [Supplementary Material](#). The F1 loop thus complements these known binding sites with an additional specific binding site, again comprising primarily lysines.

DISCUSSION AND OUTLOOK

Using atomistic MD simulations, we provide mechanistic insight into the membrane recognition dynamics of talin. Our simulations propose a new mode of interaction that helps to explain how talin can bind the membrane even when its main PIP₂ (and integrin) binding sites in F2 and F3 (20) (see figure Figure 6b) are blocked by autoinhibition (23). Specifically, we find the unique unstructured, 33-residue-long insertion into the F1 domain, the F1 loop, to provide a strong interaction anchor to PIP₂-containing membranes.

Overall, the FERM-membrane interaction mode is not characterized by singular binding sites interacting with one molecule of PIP₂ each, as would be the conclusion from crystallographic data alone. Rather the cumulative diffuse interaction of multiple PIP₂ with multiple residues is what keeps the protein anchored to the membrane. This is particularly evident in the interaction with the flexible F1 loop, but also in the F0 domain. While crystal structures of proteins in complex with PIP₂ typically show a one-to-one ratio of lipid per binding site (20, 48, 49), possibly due to the nature of the experimental method, our simulations suggest multiple PIP₂ molecules binding simultaneously. Similar results have been observed for Pleckstrin Homology (PH) domain proteins by Naughton et al. (50). According to their study, this simultaneous binding of multiple PIP₂ molecules contributes to the high affinity of the membrane interaction.

Our MD simulations suggest that the F1 loop can find favorable interactions with PIP₂ across large distances and in a large search volume. We find this to be the disordered loop's high flexibility. The F1 loop can maintain the membrane contacts when talin is pulled

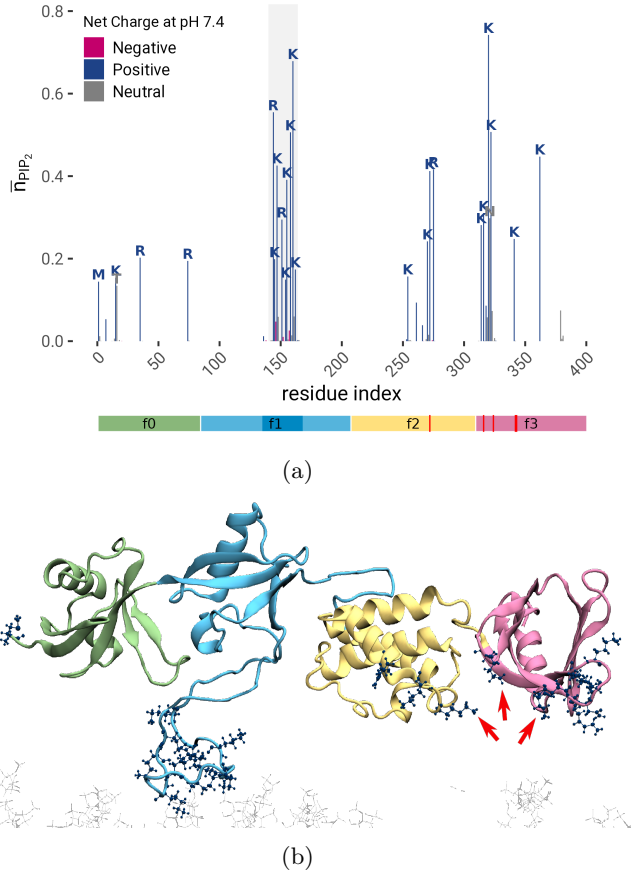


Figure 6: Simulation of the full-length FERM domain over a 10% PIP₂-membrane. **a)** The average number of PIP₂ molecules interacting with the individual residues across 6 simulations. Color represents the charge of the amino acid at pH 7.4 (blue = positive/basic, magenta = negative/acidic). The known PIP₂ interaction sites K272 of F2 and K316, K324, E342, and K343 of F3 (20) are highlighted with red lines on the x-axis colorbar and can also be seen in the cartoon representation in **b)** where the interacting residues with a score greater than 0.2 are displayed as dark blue stick models.

off of the membrane over distances as large as 7 nm. A similar mechanism has also been shown by Shoemaker et al. (51) and was fittingly coined “fly-casting”. In the aforementioned publication they focus on the interaction of unfolded regions with DNA. Our simulations now provide an example for the concept applied to protein-lipid interactions. It is well worth noting that, although we mention the greater search space of the F1 loop as its advantage in recognizing PIP₂, it has also been argued that the kinetic advantage of the fly-casting mechanism comes mainly from the reduction in free energy as the disordered region folds around the interaction target (52). This can also be argued here, as the loop can flexibly adapt its conformation to the membrane and the dynamic distribution of PIP₂ lipids therein. As such it can bind in a multivalent fashion, with several basic residues binding to several PIP₂ lipids.

Fast binding kinetics are crucial for talin’s function at focal adhesion sites. As the PIP₂ concentrations increases at the active focal adhesion site, talin’s FERM F1 loop can perform rapid recognition. The flexibility of the loop also allows it to anchor the protein at the membrane even when being stretched under force (up to a delta of 7 nm, as seen in Figure 5). This is akin to the elastic response seen in focal adhesion kinase (FAK) under force, in which a 49-residue-long linker allows for buffering of the force (53). Here, talin’s F1 loop can extend and thereby maintain the interactions, which could help rapid rebinding when the force is relieved.

In our force probe simulations, we pulled F0F1 orthogonally off the membrane. This allowed us to assess the full extension and force resistance of the loop. *In vivo*, however, talin’s FERM domain is subjected to forces acting at a 30° angle. This might imply an additional function for the FERM domain. As it is dragged along the membrane, the diffuse interactions of the F1 loop and main interaction sites in F2-F3 with PIP₂ would increase lateral friction along the membrane as the PIP₂ concentration increases. This could further localize talin at active focal adhesion sites even in the presence of forces acting parallel to the membrane.

We conclusively show that the F1 loop is able to interact with the membrane even from most unfavorable orientations. The role of the F1 loop in this is kinetic in nature. Previous studies have shown F0F1 to not significantly influence the binding equilibrium of a FERM domain to immobilized PIP₂-containing membranes compared to constructs containing only F2F3 (54). Also, when the main binding site in F2F3 was mutated, another study using lipid co-sedimentation found that the F1-loop alone does not suffice to restore lipid binding (20). Our study suggests that while the thermodynamics of binding might remain unchanged, the equilibrium should be reached faster due to the presence of the loop. We propose that talin mutants lack-

ing the loop, or specifically the basic residues in said loop, will show reduced or at least slowed-down focal adhesion maturation, increased lateral diffusion of talin under force, and faster focal adhesion disassembly. We note that given the high disorder of the F1 loop, we speculate that this interaction is rather unspecific compared to the PIP₂-specific F2F3 site, and interactions with PIP₃ are also likely to form. To what extent our conclusions are also applicable to talin-2 remains to be shown. Given the high sequence similarity and conservation of the F1 loop (13), we speculate that it plays a similar role as early PIP₂ anchor in the talin-2 isoform as well.

Recognition is only the first step. The mechanistic details of how talin’s autoinhibition is resolved remain to be shown by larger simulations including the inhibiting rod segment. These larger-scale simulations might then be able to provide evidence for the push-pull mechanism proposed by Song et al. (12) or might reveal how the early F1-loop mediated membrane interactions identified in this study might effect the subsequent steps for talin activation.

As the F1-loop has been shown to contribute to integrin activation (13), it will also be insightful to simulate a system including the integrin tail. This is a promising approach, since other computational studies have also found PIP₂ to be crucial, not just for the membrane interaction, but also the formation of the protein–protein complex. The cloverleaf-like FERM domain of moesin, for example, interacts with the cytoplasmic domain of L-selectin mediated by PIP₂ (55) and PIP₂ enables the formation of the CD44-FERM complex for radixin (56).

In conclusion, we propose positively charged, intrinsically disordered regions in talin’s FERM domain and potentially other PIP₂-binding domains to promote fast recognition and to help maintain the membrane interaction under force.

AUTHOR CONTRIBUTIONS

Conceived and designed the experiments: JB FF FG. Performed the experiments: JB FF. Analyzed the data: JB FF. Contributed reagents/materials/analysis tools: FF. Wrote the paper: JB FF.

DECLARATION OF INTERESTS

The authors declare no competing interests.

ACKNOWLEDGMENTS

This work was supported by the Klaus Tschira Foundation and the European Research Council (ERC) under the European Union’s Horizon 2020 research and innovation programme (grant agreement No. 101002812).

REFERENCES

1. Vogel, V., and M. Sheetz. 2006. Local force and geometry sensing regulate cell functions. *Nature Reviews Molecular Cell Biology*. 7:265–275.
2. Oakes, P.W., and M.L. Gardel. 2014. Stressing the limits of focal adhesion mechanosensitivity. *Current Opinion in Cell Biology*. 30:68–73.
3. Schiller, H.B., and R. Fässler. 2013. Mechanosensitivity and compositional dynamics of cell-matrix adhesions. *EMBO reports*. 14:509–519.
4. Miroshnikova, Y.A., H.Q. Le, D. Schneider, T. Thalheim, M. Rübsam, N. Bremicker, J. Polleux, N. Kamprad, M. Tarantola, I. Wang, M. Balland, C.M. Niessen, J. Galle, and S.A. Wickström. 2018. Adhesion forces and cortical tension couple cell proliferation and differentiation to drive epidermal stratification. *Nature Cell Biology*. 20:69–80.
5. Thamilselvan, V., and M.D. Basson. 2004. Pressure activates colon cancer cell adhesion by inside-out focal adhesion complex and actin cytoskeletal signaling. *Gastroenterology*. 126:8–18.
6. Pelletier, A.J., T. Kunicki, Z.M. Ruggeri, and V. Quaranta. 1995. The Activation State of the Integrin $\alpha IIb\beta 3$ Affects Outside-in Signals Leading to Cell Spreading and Focal Adhesion Kinase Phosphorylation *. *Journal of Biological Chemistry*. 270:18133–18140.
7. Yao, M., B.T. Goult, B. Klapholz, X. Hu, C.P. Toseland, Y. Guo, P. Cong, M.P. Sheetz, and J. Yan. 2016. The mechanical response of talin. *Nature Communications*. 7:11966.
8. Tadokoro, S., S.J. Shattil, K. Eto, V. Tai, R.C. Liddington, J.M. de Pereda, M.H. Ginsberg, and D.A. Calderwood. 2003. Talin Binding to Integrin β Tails: A Final Common Step in Integrin Activation. *Science*. 302:103–106.
9. Chishti, A.H., A.C. Kim, S.M. Marfatia, M. Lutchman, M. Hanspal, H. Jindal, S.-C. Liu, P.S. Low, G.A. Rouleau, N. Mohandas, J.A. Chassis, J.G. Conboy, P. Gascard, Y. Takakuwa, S.-C. Huang, E.J.B. Jr, A. Bretscher, R.G. Fehon, J.F. Gusella, V. Ramesh, F. Solomon, V.T. Marchesi, S. Tsukita, S. Tsukita, M. Arpin, D. Louvard, N.K. Tonks, J.M. Anderson, A.S. Fanning, P.J. Bryant, D.F. Woods, and K.B. Hoover. 1998. The FERM domain: A unique module involved in the linkage of cytoplasmic proteins to the membrane. *Trends in Biochemical Sciences*. 23:281–282.
10. Mani, T., R.F. Hennigan, L.A. Foster, D.G. Conrady, A.B. Herr, and W. Ip. 2011. FERM Domain Phosphoinositide Binding Targets Merlin to the Membrane and Is Essential for Its Growth-Suppressive Function. *Molecular and Cellular Biology*. 31:1983–1996.
11. Das, T., K. Safferling, S. Rausch, N. Grabe, H. Boehm, and J.P. Spatz. 2015. A molecular mechanotransduction pathway regulates collective migration of epithelial cells. *Nature Cell Biology*. 17:276–287.
12. Song, X., J. Yang, J. Hirbawi, S. Ye, H.D. Perera, E. Goksoy, P. Dwivedi, E.F. Plow, R. Zhang, and J. Qin. 2012. A novel membrane-dependent on/off switch mechanism of talin FERM domain at sites of cell adhesion. *Cell Research*. 22:1533–1545.
13. Goult, B.T., M. Bouaouina, P.R. Elliott, N. Bate, B. Patel, A.R. Gingras, J.G. Grossmann, G.C.K. Roberts, D.A. Calderwood, D.R. Critchley, and I.L. Barsukov. 2010. Structure of a double ubiquitin-like domain in the talin head: A role in integrin activation. *The EMBO Journal*. 29:1069–1080.
14. Elliott, P.R., B.T. Goult, P.M. Kopp, N. Bate, J.G. Grossmann, G.C.K. Roberts, D.R. Critchley, and I.L. Barsukov. 2010. The Structure of the Talin Head Reveals a Novel Extended Conformation of the FERM Domain. *Structure(London, England:1993)*. 18:1289–1299.
15. Calderwood, D.A., R. Zent, R. Grant, D.J.G. Rees, R.O. Hynes, and M.H. Ginsberg. 1999. The Talin Head Domain Binds to Integrin β Subunit Cytoplasmic Tails and Regulates Integrin Activation *. *Journal of Biological Chemistry*. 274:28071–28074.
16. Calderwood, D.A., I.D. Campbell, and D.R. Critchley. 2013. Talins and kindlins: Partners in integrin-mediated adhesion. *Nature Reviews Molecular Cell Biology*. 14:503–517.
17. Horwitz, A., K. Duggan, C. Buck, M.C. Beckerle, and K. Burridge. 1986. Interaction of plasma membrane fibronectin receptor with talin—a transmembrane linkage. *Nature*. 320:531–533.
18. McCann, R.O., and S.W. Craig. 1997. The I/LWEQ module: A conserved sequence that signifies F-actin binding in functionally diverse proteins from yeast to mammals. *Proceedings of the National Academy of Sciences*. 94:5679–5684.
19. Klapholz, B., and N.H. Brown. 2017. Talin – the master of integrin adhesions. *Journal of Cell Science*. 130:2435–2446.

20. Chinthalapudi, K., E.S. Rangarajan, and T. Izard. 2018. **The interaction of talin with the cell membrane is essential for integrin activation and focal adhesion formation.** *Proceedings of the National Academy of Sciences of the United States of America.* 115:10339–10344.
21. Saltel, F., E. Mortier, V.P. Hytönen, M.-C. Jacquier, P. Zimmermann, V. Vogel, W. Liu, and B. Wehrle-Haller. 2009. **New PI(4,5)P₂- and membrane proximal integrin-binding motifs in the talin head control B3-integrin clustering.** *Journal of Cell Biology.* 187:715–731.
22. Banno, A., B.T. Goult, H. Lee, N. Bate, D.R. Critchley, and M.H. Ginsberg. 2012. **Subcellular Localization of Talin Is Regulated by Inter-domain Interactions ***. *Journal of Biological Chemistry.* 287:13799–13812.
23. Dedden, D., S. Schumacher, C.F. Kelley, M. Zacharias, C. Biertümpfel, R. Fässler, and N. Mizuno. 2019. **The Architecture of Talin1 Reveals an Autoinhibition Mechanism.** *Cell.* 179:120–131.e13.
24. Buyan, A., A.C. Kalli, and M.S.P. Sansom. 2016. **Multiscale Simulations Suggest a Mechanism for the Association of the Dok7 PH Domain with PIP-Containing Membranes.** *PLOS Computational Biology.* 12:e1005028.
25. Zhou, J., C. Aponte-Santamaría, S. Sturm, J.T. Bullerjahn, A. Bronowska, and F. Gräter. 2015. **Mechanism of Focal Adhesion Kinase Mechanosensing.** *PLOS Computational Biology.* 11:e1004593.
26. Berendsen, H.J.C., D. van der Spoel, and R. van Drunen. 1995. **GROMACS: A message-passing parallel molecular dynamics implementation.** *Computer Physics Communications.* 91:43–56.
27. Abraham, M.J., T. Murtola, R. Schulz, S. Páll, J.C. Smith, B. Hess, and E. Lindahl. 2015. **GROMACS: High performance molecular simulations through multi-level parallelism from laptops to supercomputers.** *SoftwareX.* 1–2:19–25.
28. Lindahl, Abraham, Hess, and van der Spoel. 2020-01-01, 2020-01. **GROMACS 2020 source code.** Zenodo.
29. Martí-Renom, M.A., A.C. Stuart, A. Fiser, R. Sánchez, F. Melo, and A. Sali. 2000. **Comparative protein structure modeling of genes and genomes.** *Annual Review of Biophysics and Biomolecular Structure.* 29:291–325.
30. Webb, B., and A. Sali. 2016. **Comparative Protein Structure Modeling Using MODELLER.** *Current Protocols in Protein Science.* 86:2.9.1–2.9.37.
31. Pettersen, E.F., T.D. Goddard, C.C. Huang, G.S. Couch, D.M. Greenblatt, E.C. Meng, and T.E. Ferrin. 2004. **UCSF Chimera—a visualization system for exploratory research and analysis.** *Journal of Computational Chemistry.* 25:1605–1612.
32. Brooks, B.R., C.L. Brooks, A.D. Mackerell, L. Nilsson, R.J. Petrella, B. Roux, Y. Won, G. Archontis, C. Bartels, S. Boresch, A. Caflisch, L. Caves, Q. Cui, A.R. Dinner, M. Feig, S. Fischer, J. Gao, M. Hodoscek, W. Im, K. Kuczera, T. Lazaridis, J. Ma, V. Ovchinnikov, E. Paci, R.W. Pastor, C.B. Post, J.Z. Pu, M. Schaefer, B. Tidor, R.M. Venable, H.L. Woodcock, X. Wu, W. Yang, D.M. York, and M. Karplus. 2009. **CHARMM: The biomolecular simulation program.** *Journal of Computational Chemistry.* 30:1545–1614.
33. Jo, S., T. Kim, V.G. Iyer, and W. Im. 2008. **CHARMM-GUI: A web-based graphical user interface for CHARMM.** *Journal of Computational Chemistry.* 29:1859–1865.
34. Lee, J., X. Cheng, J.M. Swails, M.S. Yeom, P.K. Eastman, J.A. Lemkul, S. Wei, J. Buckner, J.C. Jeong, Y. Qi, S. Jo, V.S. Pande, D.A. Case, C.L. Brooks, A.D. MacKerell, J.B. Klauda, and W. Im. 2016. **CHARMM-GUI Input Generator for NAMD, GROMACS, AMBER, OpenMM, and CHARMM/OpenMM Simulations Using the CHARMM36 Additive Force Field.** *Journal of Chemical Theory and Computation.* 12:405–413.
35. Hoover, W.G. 1985. **Canonical dynamics: Equilibrium phase-space distributions.** *Physical Review A.* 31:1695–1697.
36. Nosé, S. 1984. **A unified formulation of the constant temperature molecular dynamics methods.** *The Journal of Chemical Physics.* 81:511–519.
37. Parrinello, M., and A. Rahman. 1981. **Polymorphic transitions in single crystals: A new molecular dynamics method.** *Journal of Applied Physics.* 52:7182–7190.
38. McLaughlin, S., J. Wang, A. Gambhir, and D. Murray. 2002. **PIP2 and Proteins: Interactions, Organization, and Information Flow.** *Annual Review of Biophysics and Biomolecular Structure.* 31:151–175.
39. Mercadante, D., F. Gräter, and C. Daday. 2018. **CONAN: A Tool to Decode Dynamical Information from Molecular Interaction Maps.** *Biophysical Journal.* 114:1267–1273.

40. Landau, W.M. 2021. The targets R package: A dynamic Make-like function-oriented pipeline toolkit for reproducibility and high-performance computing. *Journal of Open Source Software*. 6:2959.
41. Wickham, H. 2016. Ggplot2: Elegant graphics for data analysis. Springer-Verlag New York.
42. Sehnal, D., S. Bittrich, M. Deshpande, R. Svobodová, K. Berka, V. Bazgier, S. Velankar, S.K. Burley, J. Koča, and A.S. Rose. 2021. Mol* Viewer: Modern web app for 3D visualization and analysis of large biomolecular structures. *Nucleic Acids Research*. 49:W431–W437.
43. Community, B.O. 2018. Blender - a 3D modelling and rendering package.
44. Humphrey, W., A. Dalke, and K. Schulten. 1996. VMD – Visual Molecular Dynamics. *Journal of Molecular Graphics*. 14:33–38.
45. Allaire, J.J., C. Teague, C. Scheidegger, Y. Xie, and C. Dervieux. 2022. Quarto.
46. Xie, Y. 2015. Dynamic documents with R and knitr. Second. Boca Raton, Florida: Chapman and Hall/CRC.
47. Aden-Buie, G. 2022. Betterposter: A better scientific poster.
48. Chinthalapudi, K., V. Mandati, J. Zheng, A.J. Sharff, G. Bricogne, P.R. Griffin, J. Kissil, and T. Izard. 2018. Lipid binding promotes the open conformation and tumor-suppressive activity of neurofibromin 2. *Nature Communications*. 9:1338.
49. Jian, X., W.-K. Tang, P. Zhai, N.S. Roy, R. Luo, J.M. Gruschus, M.E. Yohe, P.-W. Chen, Y. Li, R.A. Byrd, D. Xia, and P.A. Randazzo. 2015. Molecular Basis for Cooperative Binding of Anionic Phospholipids to the PH Domain of the Arf GAP ASAP1. *Structure*. 23:1977–1988.
50. Naughton, F.B., A.C. Kalli, and M.S.P. Sansom. 2018. Modes of Interaction of Pleckstrin Homology Domains with Membranes: Toward a Computational Biochemistry of Membrane Recognition. *Journal of Molecular Biology*. 430:372–388.
51. Shoemaker, B.A., J.J. Portman, and P.G. Wolynes. 2000. Speeding molecular recognition by using the folding funnel: The fly-casting mechanism. *Proceedings of the National Academy of Sciences of the United States of America*. 97:8868–8873.
52. Huang, Y., and Z. Liu. 2009. Kinetic Advantage of Intrinsically Disordered Proteins in Coupled Folding–Binding Process: A Critical Assessment of the “Fly-Casting” Mechanism. *Journal of Molecular Biology*. 393:1143–1159.
53. Bauer, M.S., F. Baumann, C. Daday, P. Redondo, E. Durner, M.A. Jobst, L.F. Milles, D. Mercadante, D.A. Pippig, H.E. Gaub, F. Gräter, and D. Lietha. 2019. Structural and mechanistic insights into mechanoactivation of focal adhesion kinase. *Proceedings of the National Academy of Sciences*. 116:6766–6774.
54. Moore, D.T., P. Nygren, H. Jo, K. Boesze-Battaglia, J.S. Bennett, and W.F. DeGrado. 2012. Affinity of talin-1 for the B3-integrin cytosolic domain is modulated by its phospholipid bilayer environment. *Proceedings of the National Academy of Sciences*. 109:793–798.
55. Sun, F., C.F.E. Schroer, L. Xu, H. Yin, S.J. Marrink, and S.-Z. Luo. 2018. Molecular Dynamics of the Association of L-Selectin and FERM Regulated by PIP2. *Biophysical Journal*. 114:1858–1868.
56. Sun, F., C.F.E. Schroer, C.R. Palacios, L. Xu, S.-Z. Luo, and S.J. Marrink. 2020. Molecular mechanism for bidirectional regulation of CD44 for lipid raft affiliation by palmitoylations and PIP2. *PLOS Computational Biology*. 16:e1007777.

SUPPLEMENTARY MATERIAL

Simulation Systems and Structures

These interactive displays are available in the web version: <https://hits-mbm-dev.github.io/paper-talin-loop/>

Scripts

Data analysis code is available at https://hits-mbm-dev.github.io/paper-talin-loop/_analysis.html and in the repository at <https://github.com/hits-mbm-dev/paper-talin-loop>.

Input files and raw data

Input files and raw data are available on [heiData](#) here:
<https://doi.org/10.11588/data/BQTQUN>

Supplementary Plots and Tables

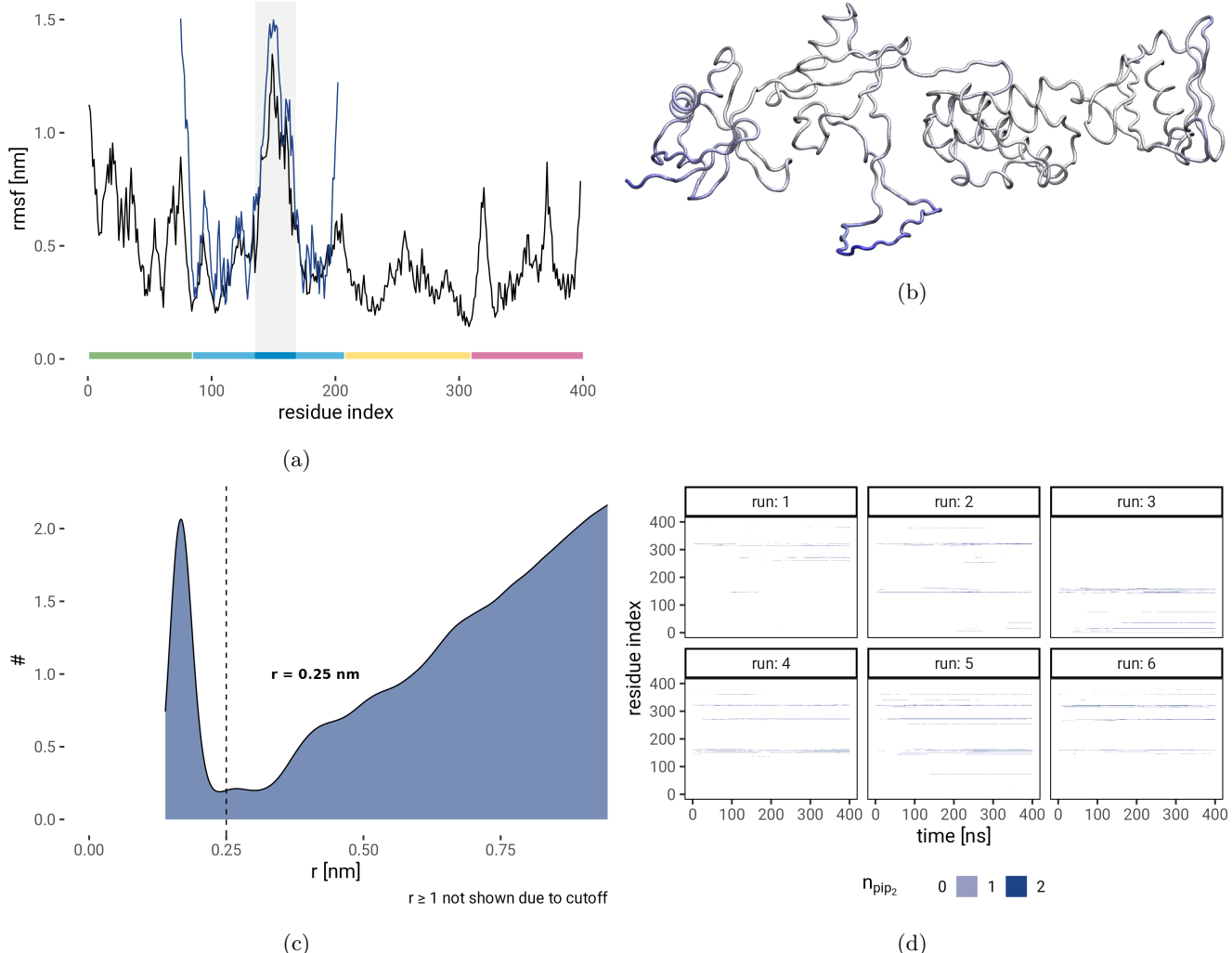


Figure 7: **a)** Root Mean Squared Fluctuation (RMSF) per residue in an equilibrium simulation of the full-length FERM domain (black). The additional blue line shows the RMSF of the NMR ensemble of F1 for comparison (2KC2 (13)). The region of the loop in F1 is highlighted by a grey shade. Color bars as in Figure 6b. **b)** The relative magnitude of the RMSF is shown by coloring the backbone in a render of the FERM structure. **c)** Density plot of distances between PIP₂ and the protein residues to decide on a cutoff for defining interactions. A distance of 0.25 nm was chosen. **d)** A heatmap of the number of PIP₂ molecules bound per residue over time for the 6 individual simulations with the whole FERM domain over the membrane.

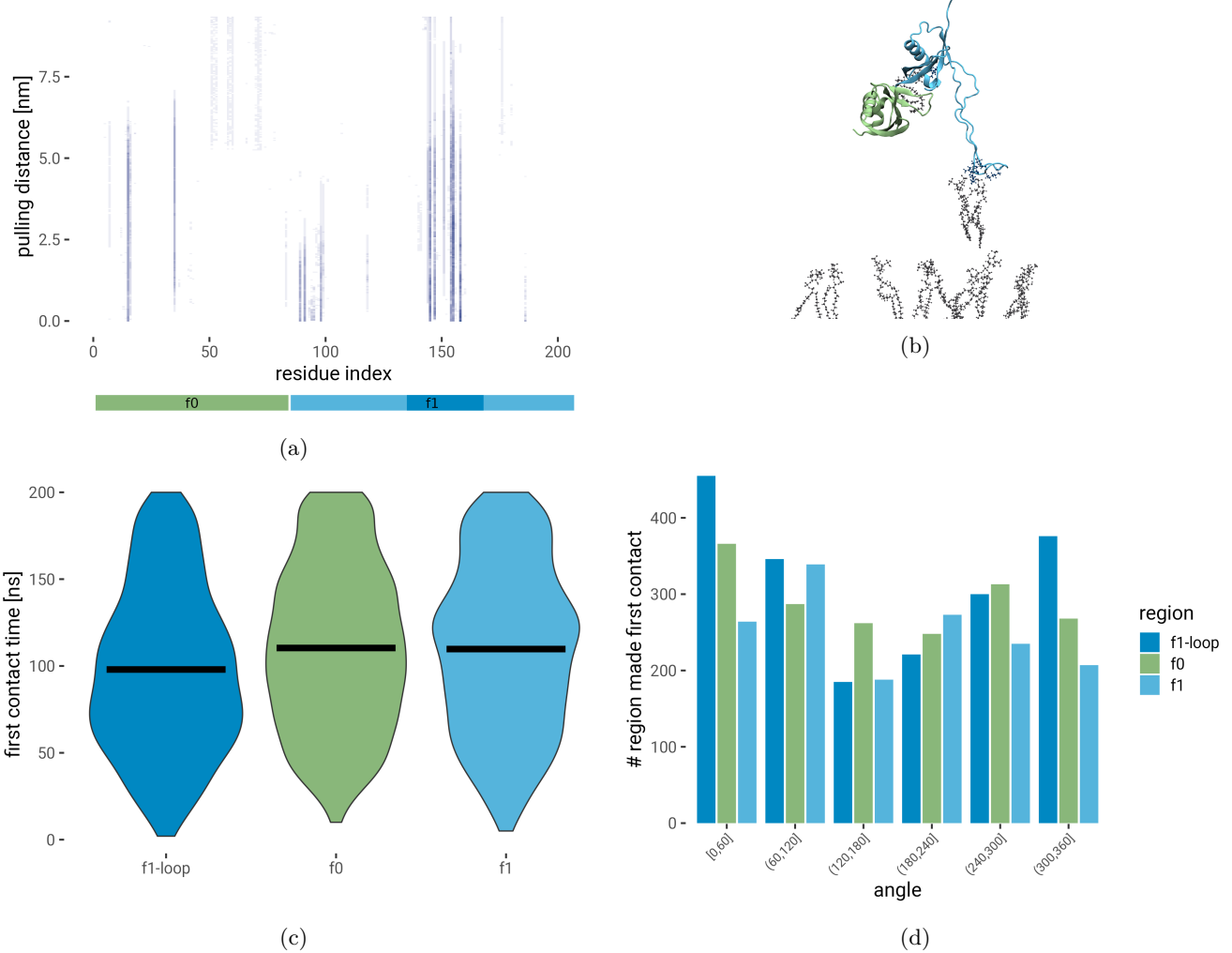


Figure 8: **a)** A closer look at the residues involved in the interaction during pulling reveals the instrumental role of both the F1 loop as well as the F0 subdomain in keeping the connection to the membrane. **b)** Run 4 of the vertical pulling of F0F1. Interactions between the protein and PIP₂ were so strong that a total of 3 molecules of PIP₂ (gray) were pulled out of the membrane (1 by F0 (green) and 2 by the F1 loop (blue)). **c)** Time to first contact of a residue with PIP₂ in the rotational sampling of F0F1. Residues belonging to the F1 loop on average make contact earlier. **d)** Number of times a residue belonging to a region made the first contact in the rotational sampling of F0F1.

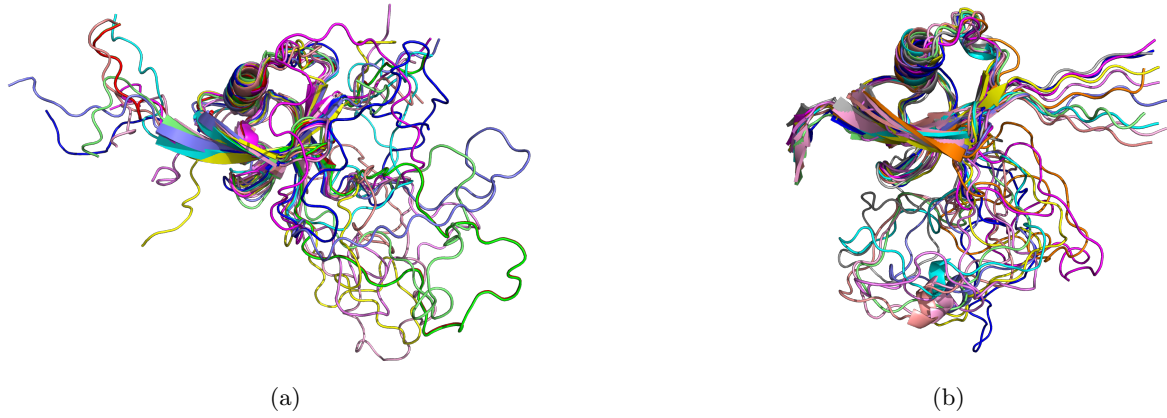


Figure 9: **a)** NMR ensemble of F1, pdb ID 2KC2 ([13](#)) **b)** Ensemble of the F1 domain in equilibrium simulations of the completed FERM domain. The other domains (F0,F2,F3) are not shown, but their steric influence can be seen, as the flexible loop can now no longer occupy the space of the F2 domain as in the NMR structure in **a**.

Table 1: Top residues interacting with F0F1

| residue | mean_n_pip |
|---------|------------|
| M 1 | 0.118 |
| K 15 | 0.114 |
| R 30 | 0.104 |
| R 35 | 0.155 |
| K 98 | 0.101 |
| R 118 | 0.127 |
| R 144 | 0.179 |
| K 147 | 0.155 |
| R 151 | 0.209 |
| K 154 | 0.144 |
| K 155 | 0.152 |
| K 158 | 0.154 |
| K 160 | 0.139 |
| K 162 | 0.107 |
| R 193 | 0.120 |

Table 2: Top residues interacting with FERM

| residue | mean_n_pip |
|---------|------------|
| M 1 | 0.144 |
| K 15 | 0.154 |
| T 16 | 0.134 |
| R 35 | 0.202 |
| R 74 | 0.195 |
| R 144 | 0.555 |
| K 145 | 0.199 |
| K 147 | 0.426 |
| R 151 | 0.295 |
| K 154 | 0.149 |
| K 155 | 0.391 |
| K 158 | 0.506 |
| K 160 | 0.679 |
| K 162 | 0.174 |
| K 254 | 0.157 |
| K 270 | 0.242 |
| K 272 | 0.412 |
| R 275 | 0.416 |
| K 314 | 0.281 |
| K 316 | 0.310 |
| K 320 | 0.742 |
| N 321 | 0.298 |
| K 322 | 0.507 |
| K 341 | 0.248 |
| K 362 | 0.447 |

Molecular dynamics Parameters

Production runs

```
integrator          = md
dt                 = 0.002
nsteps             = 100000000
cutoff-scheme      = Verlet
nstlist             = 20
rlist               = 1.2
coulombtype        = pme
rcoulomb            = 1.2
vdwtype            = Cut-off
vdw-modifier       = Force-switch
rvdw_switch         = 1.0
rvdw                = 1.2
tcoupl              = Nose-Hoover
tc_grps             = SYSTEM
tau_t               = 1.0
ref_t               = 303.15
pcoupl              = Parrinello-Rahman
pcoupltype          = semiisotropic
tau_p               = 5.0
compressibility     = 4.5e-5 4.5e-5
ref_p               = 1.0    1.0
constraints          = h-bonds
constraint_algorithm = LINCS
continuation         = yes
nstcomm              = 100
comm_mode            = linear
comm_grps            = SYSTEM
refcoord_scaling     = com
```